Confinement effect on hydrolysis in small lipid vesicles

Ben Woods, Katherine Thompson, Nicolas Szita, Shu Chen, Lilia Milanesi, Salvador Tomas

Section 1. Experimental methods

Instrumentation, materials and reagents

Chemicals and solvents were purchased from commercial sources and used without further purification. UV-Vis absorbance spectra were recorded with Thermo Scientific Evolution 201 UV-Visible spectrophotometer, equipped with a Smart Thermostatted Rotary System 7-Cell Changer and Fisherbrand Isotemp Refrigerated Bath Circulator. Fluorescence emission spectra were recorded with a Hitachi F-7000 Spectrophotometer. ^{1}H NMR spectra was recorded using a Bruker Advance Neo 700 instrument. Dynamic light scattering (DLS) measurements were recorded using an Unchained Labs Punk D 0037 Dynamic Light Scattering Analyser.

Kinetic, size distribution and lipid binding experiments were carried out at a temperature of 37 C in sodium phosphate buffer 100 mM, NaCl 2 M, pH = 7.2. For osmotic shock experiments the vesicles were prepared in in sodium phosphate buffer 100 mM, pH = 7.2. The concentration of NaCl was then brought up to 2 M during the osmotic shock procedure. See "*Osmotically shrunk liposome kinetic experiment"* below.

Synthesis of 8-acetoxypyrene-1,3,6-trisulfonate (AP)

Synthesis of **AP** was carried out according to a previous reported procedure.[25] Briefly, sodium acetate (2 mg, 24 µmol, 0.12 eq.) was dissolved in acetic anhydride (1.2 mL). Pyranine (105 mg, 0.2 mmol , 1 eq.) was added to the clear solution. The yellow suspension was heated at 140°C for 18 h, after which the suspension was allowed to cool to room temperature and the off white suspension was filtered. The precipitate was washed first with cold acetone (approx. 1-2 mL), and then excess cold diethylether to give the pure product, 8-acetoxypyrene-1,3,6-trisulfonate (AP) as an off white powder (98 mg, 0.17 mmol, 85 %). 1H NMR (700 mHz, DMSO-d6):9.12 (s, 1H), 9.08 (d, *J* = *J* = 9.6 Hz, 1H), 8,96 (d, *J* = 9.8 Hz, 1H), 8,89 (d, *J* = 9,8 Hz, 1H), 8,73 (d, *J* = 9,6 Hz, 1H), 8,27 (s, 1H), 2.17 (s, 3H) ppm.

Liposome samples. Ethanolic stock solutions of dioleoyl phosphatidylcholine (DOPC, 30 mM) and methyldioctadecylammonium bromide DODAB (10 mM) were prepared. Aliquots of the lipid stock solutions (calculated depending on the final desired lipid composition) were mixed and evaporated under reduced pressure for at least 30 minutes. The lipid film was suspended in buffer to give a final total lipid concentration of 2 mM. The liposome suspension was extruded 21 times through polycarbonate filters of the appropriate pore size (either 400 or 50 nm) to produce a stock solution of lipid vesicles (2 mM). These samples were used to test the influence of lipid vesicles on the hydrolysis of non-confined AP and to evaluate the binding of **AP** to the lipid membrane.

Liposomes loaded with AP. To generate lipid vesicle samples containing encapsulated **AP**, the lipid film was suspended in the appropriate buffer containing **AP** (5 mM), to a final lipid concentration of 5 mM. The liposome suspension was extruded 21 times through polycarbonate filters of the appropriate size to produce lipid vesicle stock solution (see the

section *Lipid Vesicle Sizes* below for more details). 1 mL of this suspension was then applied to a gel permeation chromatography column, loaded with Sepharose 4B (size of the bed 1.5 x 15 cm), in order to remove non-confined **AP** (except for samples S1, see *Lipid Vesicle Sizes* below for more details). The liposomes were collected in approximately 2 mL of eluate, yielding a final concentration of lipids of approximately 2.5 mM. Samples with smallest vesicle size where generated by subjecting suspensions of lipid vesicles obtained by extrusion through a 50 nm pore size polycarbonate filter to 9 min of sonication with ultrasonic probe. Excess **AP** was then removed by gel permeation chromatography.

Kinetic experiments.

Liposome size kinetic experiment: In a typical experiment, a set of 6 samples were prepared at a given lipid composition. Sample S0 contained **AP** 15 μM in buffer. Samples S2 to S5 contained **AP** encapsulated in liposomes of decreasing size (Table 1). UV-Vis spectra of each sample set were taken at various time intervals over a period of 60 to 80 h.

Osmotically shrunk liposome kinetic experiment: In a typical experiment, a sample of **AP** dissolved in buffer sodium phosphate 100 mM, pH 7.2, was encapsulated in lipid vesicles, produced by extrusion through a 400 nm pore polycarbonate filter. The resulting lipid vesicles sample had an average radius of 110 nm according to DLS, with a concentration of lipids 2 mM. 500 μL of a buffer with very high salt content (sodium phosphate, 100 mM, NaCl = 4 M, pH = 7.2) was then added to 500 μL of the sample, to a final sample composed of osmotically shrunk liposomes containing **AP** (total lipids ~ 1 mM), in our normal working buffer (e.g., 100 mM sodium phosphate, 2M NaCl, pH 7.2) (sample S6). UV-Vis spectra were taken at various time intervals over a period of 60 to 120 h.

Membrane binding experiments. Experiments were conducted using UV spectroscopy. In a typical experiment, 12 samples containing a constant concentration of **AP** and increasing concentrations of liposomes in high salt buffer were prepared. The concentration of **AP** was 15 μM. The concentration of lipid ranged from 10 to 48,000 μM. After preparation, the samples were left to equilibrate for a minimum of 30 minutes and their spectrum was recorded. The experiments were carried out at 37 C.

Fluorescence quenching experiments. A solution of membrane impermeable DPX 100 mM in buffer was prepared. Aliquots of the relevant samples used for the kinetic experiments (S1 to S6) were taken and diluted 50 fold in buffer, yielding a sample of 1000 μL, and their fluorescence emission spectrum (ex. 371 nm) was recorded. Then, 150 μL of DPX solution was added and the fluorescence emission spectrum was recorded again. In these conditions photo-bleaching was negligible and all reduction in fluorescence intensity could be attributed to the effect of the DPX quenching of the **AP** fluorescence.

Dynamic light scattering experiments. Measurements were recorded in a plastic cuvette. Samples were diluted to a measurable scattering intensity and recorded at 20°C.

Cryo-Electron Microscopy Imaging. Samples were prepared inside the chamber of an automatic plunge freezer Leica GP2 kept at 20C and 90% humidity. 10 μL of sample were applied on holey carbon grids (300–400 mesh Cu, Agar-Scientific) (type of grids) previously glow discharged using PELCO easyGlow. Grids were then vitrified in liquid ethane after 5s back blotting and at 0.2mm advance distance. Images were taken using a Tecnai F20 FEG electron

microscope operated at 200 kV and collected with a K2 direct electron detector (Gatan) at a magnification of 11500x corresponding to a physical pixel size of 0.3196 nm. A Low dose setting was used: the dose rate was 8.66 e/pixel per second equivalent to 0.0.8478 e/A^2 per second and resulting in a total dose of 10.17 e/A^2 (acquisition time was 8s). Each micrograph has 60 frames and ismotion corrected and converted to tiff with scale bar

UV Data processing.

All the UV spectra where exported as ASCII data for processing with Microsoft Excel. The scattering of the lipid vesicles fits well to a third degree polynomial. Therefore, in order to remove both random baseline variations and the contribution of the lipid vesicle scattering to the absorbance, a triple derivative was applied to the spectral data. The first derivative was carried out graphically, by calculating the average of 5 contiguous data and subtracting the average of 5 contiguous data 5 nanometres apart (for example, derivative = average (A_{365}, A_{366}, A_{367}, A_{368}, A_{369}) – average (A_{360}, A_{361}, A_{362}, A_{363}, A_{364}). The second and third derivative of the absorbance, *A''* and *A'''*, where calculated by repeating the process over the results from the first derivative and second derivative respectively (Supplementary Fig S1 and S3). This procedure smooths out noise and ensures that only variations in the spectral bands relating to chemical changes in **AP** (i.e., binding or hydrolysis) are reflected in the data. [1S]

2. Characterization of the vesicles

2.1. Binding affinity of AP for the lipid membrane.

The binding affinity of **AP** for the lipid membranes was estimated using a UV spectroscopy titration method, where the UV spectrum of **AP** in buffer was recorded in solutions with increasing concentration of lipid. The experiments were designed such that the concentration of **AP** was kept constant in all the samples. The third derivative of the spectra remove the effect of lipid scattering and are therefore attributed to the absorption of **AP** free in solution and **AP** associated with the membrane (Supplementary Fig. S1). Assuming that **AP** and the lipid molecules form a complex of 1 to 1 stoichiometry, the apparent dissociation constant between the lipids and **AP**, $K_{\mathbf{d}}$, can be determined by fitting the experimental data to the following system of equations:

$$K_d = \frac{[AP][L]}{[AP \cdot L]} \qquad \text{(S1)}$$

$$[AP]_0 = [AP \cdot L] + [AP] \qquad \text{(S2)}$$

$$[L]_0 = [AP \cdot L] + [L] \qquad \text{(S3)}$$

$$A_s = \varepsilon_{s,AP}[AP] + \varepsilon_{s,\,AP \cdot L}[AP \cdot L] \qquad \text{(S4)}$$

where $[L]_0$ is the total concentration of lipid on the outer membrane leaflet (i.e., half the total lipid, which is the only lipid accessible to membrane impermeable **AP**), [**AP**•*L*] the concentration of **AP** associated with the lipids, $[\mathbf{AP}]_0$ the total concentration of **AP**, [*L*] the concentration of free lipids on the outer membrane leaflet. A_s is the sum of the third derivative of the absorbance between 372 and 377 nm minus the sum of the third derivative of the absorbance between 362 and 370 nm, i.e.

$$A_s = \sum_{i=362}^{i=370} A'''_i - \sum_{i=372}^{i=377} A'''_i \qquad \text{(S5)}$$

In our experiments, it is observed that the third derivative of the absorbance between 362 and 370 increases with binding while that between 372 and 377 decreases. The difference between the sums of each interval is therefore very sensitive to spectral changes upon binding

and enhances the signal over noise ratio. ε_s refers, similarly, to the differences of the sums of the third derivative of the corresponding extinction coefficients. Only the data for membranes with a 10% DODAB showed the necessary binding saturation to allow calculating K_d with any degree of confidence. The experimental data for these vesicles was fitted to this model using the program Origin 8.0, which allowed us to determine K_d and the extinction coefficients as parameters of the fitting (Supplementary Fig. S1). The value of the dissociation constant obtained was:

$K_d = 17 \pm 4.5\ mM$

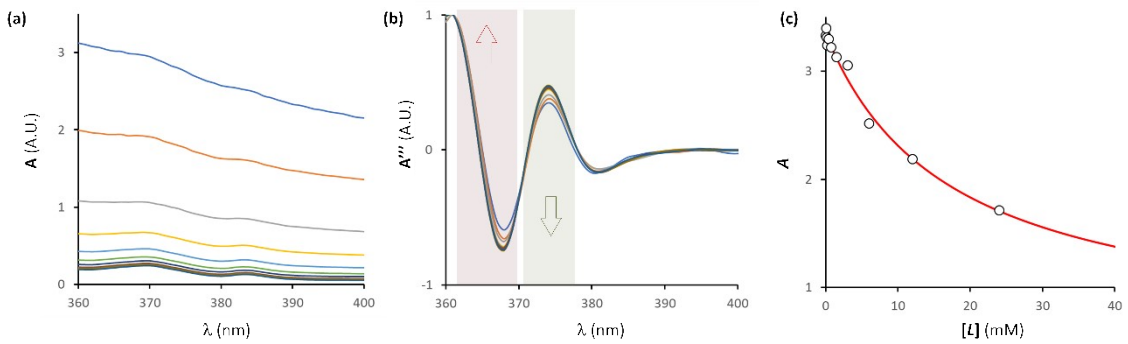

Supplementary Fig S1. (a) Changes in the UV spectrum of **AP** (15 μM) upon addition of DOPC vesicles with a 110 nm radius (the concentration of DOPC increases from 10 μM to 48 mM). (b) Third derivative of the same spectra, generated according to the procedure described in Section 1. The shadowed areas indicate the range of wavelengths whose sums were used for the data fitting as detailed in Section 2.1. (c) Sums of the third derivative of the spectra (empty circle, see eq. S5) and best fit to the binding model defined by equations S1-S4 (red trace).

2.2. Lipid Vesicle Size

The size of the lipid vesicles was controlled, in a first approximation, by the pore size of the filter used during the extrusion step of vesicle formation or by sonication (Supplementary Table S1). For samples S2 to S5 (filter pore sizes from 400 to 50 nm and sonicated), excess of non-encapsulated **AP** was removed by GPC (see Section 1, 'Liposome preparation'). Samples extruded through an 800 nm filter (S1) could not be purified using GPC as most vesicles remained stuck in the head of the Sepharose 4B matrix, presumably due to their larger size. Instead, we used Vivaspin filtration devices (cut-off 10,000 Da) to remove non-encapsulated **AP**. Briefly, 1 mL of extruded sample was loaded onto the tube and the volume was reduced to 0,1 mL. The process was repeated 6 times to a dilution factor of 10^6 for non-encapsulated **AP**. DLS was then used to obtain the average size (diameter) of vesicles from the volume (or mass) distribution. For larger pore sizes, the size found by DLS is smaller than the pore diameter used. For example, the typical size for vesicles obtained by extrusion through a 800 nm filter was 300 nm (Supplementary Table S1). The size of the vesicles was similar for all lipid compositions used. From these data we obtained the average radius used in our calculations (i.e., the radius at the mid-membrane depth, *r*. Supplementary Table 1 and Fig. 3(a)) main text.

Supplementary Table S1

Sample	Extrusion pore size (nm)	Average size from volume distribution (nm)	Average vesicle radius, r_e (nm)	Average mid-membrane vesicle radius, r (nm)
S1	**800**	**300**	**150**	**148**
S2	**400**	**220**	**110**	**108**
S3	**200**	**154**	**77**	**75**
S4	**50**	**84**	**42**	**40**
S5	**Sonication**	**66**	**33**	**31**

Table S1. Liposome diameter determined via dynamic light scattering (DLS) from preparation conditions. The error is 5% of the quoted value, measured as twice the standard deviation of 5 different data. See Fig 3 (a) (main text) for a graphical representation of r_e and r.

2.3. Fraction of AP inside the liposomes in loaded vesicles samples and vesicle stability.

The relative amount of **AP** trapped within the liposome cavity, and the presence of any leakage was determined using a fluorescence quenching assay. DPX (Supplementary Fig. S2(a)) is a membrane-impermeable molecule and a quencher of the fluorescence of **AP**. Addition of DPX over non encapsulated **AP** dissolved in the high-salt buffer leads to the quenching of 80 % of the fluorescence (Supplementary Fig. S2(b)). The addition of DPX to samples of liposomes loaded with **AP** in the same buffer leads to a slight reduction of the fluorescence (Supplementary Fig. S2(c) and (d)). The percentage of encapsulated **AP** can then be calculated by comparing with the expected extent of quenching. Let's call R_Q the ratio of quenching of **AP** accessible to DPX, that is:

$$R_Q = \frac{F_{AP.DPX}}{F_{AP}} \qquad \text{(S6)}$$

Where F_{AP} and $F_{AP.DPX}$ are the fluorescence before and after addition of DPX respectively. Q is the observed ratio of quenching upon DPX addition to vesicle encapsulated AP, where F_0 is the fluorescence before addition of DPX and F_{DPX} after the addition, i.e.:

$$Q = \frac{F_{DPX}}{F_0} \qquad \text{(S7)}$$

The fluorescence after addition can be expressed as a function of the initial fluorescence, the fraction of **AP** that is outside the vesicle (x_o) and that inside the vesicle (x_i) as follows

$$F_{DPX} = F_o(R_Q x_o + x_i) \qquad \text{(S8)}$$

Combining eqs. S6 to S8 we have that:

$$x_i = \frac{Q - R_Q}{1 - R_Q} \qquad \text{(S9)}$$

x_i takes values between 0.80 and 0.98, with the most common values around 0.95 (Supplementary Fig S2 (c) to (f)). The encapsulation fraction does not change during the time interval of our experiments (up to 7 days, Supplementary Fig S2 (e) and (f)) and does not depend on the size or composition of the lipid vesicles. The amount of encapsulated AP does not change upon subjecting the samples to osmotic shock (Supplementary Fig S2 (d)). The presence of non-encapsulated **AP** is attributed to the binding of **AP** to the membrane, which carries along a small fraction of **AP** during the GPC experiment.

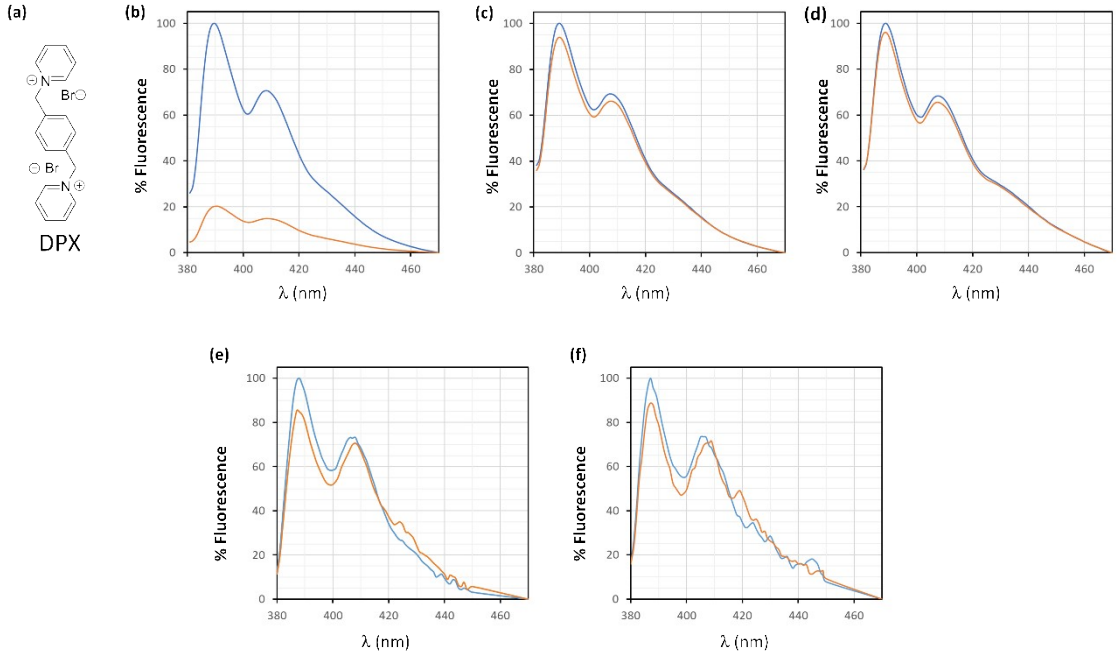

Supplementary Figure S2. (a) Chemical structure of DPX. (b) Emission fluorescence spectrum of **AP** (5 μM, excitation 371 nm) in high salt buffer (blue trace) and with the presence of 100 mM of DPX (orange trace). (c). Idem for sample S2 (i.e., AP encapsulated in vesicles extruded through a 400 nm pore filter, with 5% DODAB on the DOPC membrane). (d) idem for S6 samples (i.e., osmotically shrunk). (e). Idem for sample S5 (i.e., AP encapsulated in vesicles produced by sonication, average radius 30 nm), on a freshly produced sample after purification by GPC. (f) Idem to (e), after 4 days of hydrolysis at 37 C.

2.4. Concentration of AP inside loaded vesicles.

In the absence of any binding interaction between **AP** and the lipids, the expected amount of confined **AP** can be calculated from the initial **AP** concentration in the buffer used to prepare the liposomes, the average size of the liposomes, and the concentration of lipids. We assume an average area covered per one DOPC molecule, a_m of 0.67 nm^2.[37] Therefore, the number of molecules of DOPC per liposome, n_l, with a radius r is:

*

* For simplicity of calculations, we assume a_m to be independent of the curvature. Since the surface at the membrane mid-plain is common for both membrane leaflets, from this assumption it follows that the number of lipid molecules is the same in both leaflets, with packing defects making out for the difference in surface at the head-group depth between the inner to the outer leaflet. In reality, for high curvatures the amount of lipids is somewhat larger in the outer leaflet, as some lipids may translocate to fill-in the outer membrane defects, up to the point where the available surface at the mid-plain allow. The extreme case would have the defects in the outer leaflet fully covered by lipids that translocate from the inner leaflet. In such a scenario, the ratio of the number of lipids between the outer and inner leaflet can be estimated as the ratio between the outer and inner surfaces. For vesicles with 30 nm radius (the smallest used in this work) and a membrane 3.7 nm thick, the maximum ratio of surfaces would be 1.25. The concentration of lipids inside would therefore be around 12% lower than that calculated. The impact that this phenomenon would have in our calculations is well within the error of the measure.

$$n_l = \frac{2(4\pi r^2)}{a_m} \quad \text{(S10)}$$

If the concentration of lipids is [L], the number of liposomes per liter, N_L is

$$N_L = \frac{[L]n_a}{n_l} \quad \text{(S11)}$$

where n_a is the Avogadro number.

The combined volume of the cavities of the liposome, V_c, in one liter of solution is

$$V_C = \frac{N_L 4\pi r^3}{3} \quad \text{(S12)}$$

Assuming that the concentration of **AP** inside the liposomes is equal to that of the initial solution, i.e., [**AP**]$_{ini,}$ the expected apparent concentration of the sample, [**AP**]$_{app}$ will be

$$[AP]_{app} = V_C[AP]_{ini} \quad \text{(S13)}$$

In our typical experiment, the concentration of **AP** is 5 mM in the initial buffer, with 5 mM lipids. The lipids are then diluted after purification by GPC down to a lipid concentration of 0.5 mM. In these conditions, the expected [**AP**]$_{app}$ should be in the range of 10 to 20 μM (depending on the vesicle size used), which is consistent with the concentration on samples S1 to S6. It is therefore safe to assume that the concentration of **AP** within the confined volume of the lipid vesicle cavity is in fact 5 mM.

2.5. Concentration of lipids in the lipid vesicle cavity.

In a liposome of radius r, the concentration of lipids available for a trapped molecule is that of lipids present in the inner leaflet at any given moment. The number of lipids in the cavity, n_{lc}, can be expressed as a function of the area per lipid, a_m, and the radius r of the liposome as follows:

$$n_{lcav} = \frac{4\pi r^2}{a_m} \quad \text{(S14)}$$

while the volume of the liposome, V_L, is

$$V_L = \frac{4\pi r^3}{3} \quad \text{(S15)}$$

The concentration of lipids in the cavity, $[L]_c$, is

$$[L]_c = \frac{n_{lc}}{V_L n_A} \quad \text{(S16)}$$

Combining with eqs. S14-S16, $[L]_c$ can be expressed as a function of the radius and the area per lipid molecule as

$$[L]_c = \frac{3}{n_A a_m r} \quad (2)$$

2.6. UV kinetic experiments.

We assume that all the reactions of hydrolysis of **AP** in our experiments follow a first order kinetic law, with the integrated form:

$$[AP] = [AP]_0 e^{-kt} \quad (S17)$$

where the apparent rate constant *k* is the rate constant in a particular experiment. The third derivative of the absorbance, A''', is proportional to the concentration of the species contributing to the signal (**AP** and **P** in our case). Similarly, to what we do for the calculation of K_d, we calculate A_s, in this case as the sum of the third derivative of the absorbance between 360 and 366 nm minus the sum of the third derivative of the absorbance between 367 and 372 nm, i.e.:

$$A_s = \sum_{i=360}^{i=366} A'''_i - \sum_{i=367}^{i=372} A'''_i \quad (S18)$$

A_s can be written as a function of the concentration of **AP** and **P** as follows:

$$A_s = \varepsilon_{s,AP}[AP] + \varepsilon_{s,P}[P] \quad (S19)$$

Where ε_s are the differences of the sums of the third derivative of the corresponding extinction coefficients.

the mass balance is:

$$[AP]_0 = [AP] + [P] \quad (S20)$$

where $[\mathbf{AP}]_0$ is the initial concentration of **AP**. Combining equations S18-S20, the absorbance can be expressed as a function of the rate constant:

$$A_s = A_{s,f} - \Delta A_s e^{-kt} \quad (S21)$$

Where $A_{s,f}$ is the value of A_s upon complete hydrolysis and ΔA_s the total increase in A_s upon hydrolysis.

Eq. S21 was used to fit the data of the samples containing **AP** free in solution (i.e. samples S0). The rate constant *k* obtained from the fitting is the rate of hydrolysis of the ester bond of **AP** in the bulk of the solution, k_b (Table 1).

For all samples of vesicle encapsulated **AP** (S1 to S6) there is in all cases a small fraction of free, non-confined **AP**. The presence of vesicles at the concentration used in these experiments does not have an effect on the hydrolysis of the **AP** in the bulk. The rate constant for the hydrolysis of the non-confined fraction is therefore k_b. The change in absorbance in these samples should therefore reflect the fact that there is a fraction of vesicle confined **AP** (i.e., x_i) that hydrolyses with a rate constant *k* and a fraction of non-confined **AP** (i.e., 1-x_i) with hydrolysis rate constant k_b, that is:

$$A_s = A_{s,f} - \Delta A_s x_i e^{-kt} - \Delta A_s (1 - x_i) e^{-k_b t} \quad \text{(S22)}$$

Eq. S22 was used to fit the experimental data for all kinetic experiments. The value of x_i was determined by means of the fluorescence quenching experiment and entered as a fixed parameter, as was k_b. The fitted parameters where A_s, ΔA_s and k, the rate constant for the confined fraction (Table 1).

An example of UV spectra changes and those of the third derivative of the spectra of samples S0-S6 is shown in Supplementary Fig. S3, as well as the fitting of the A_s data to Eq. (S22). For clarity of exposition, in Fig. 2 in the main text, the absorbance differences in the y-axis have been replaced by percentage of **AP** remaining, %**AP**, using the following equation:

$$\%AP = 100\frac{A_s - A_{s,f}}{\Delta A_s} \quad \text{(S23)}$$

Using the values of $A_{s,f}$ and ΔA_s obtained from the fitting.

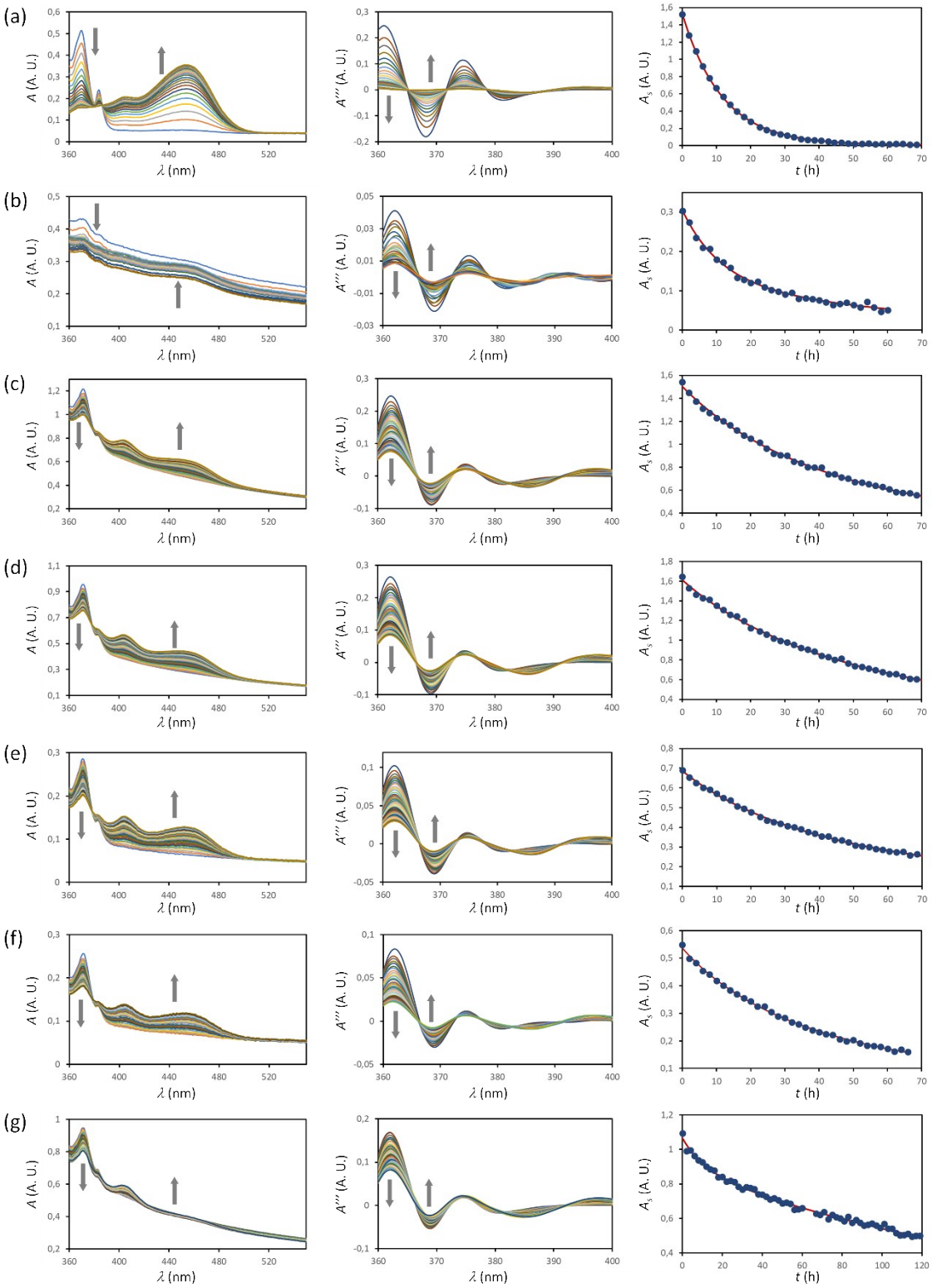

Supplementary Figure S3. (a) Left side: section of the UV spectrum of sample S0 (**AP** 15 μM on high salt buffer, pH 7.2) recorded at different times. Central panel: section of the third derivative of the spectra shown on the left panel. Right side panel: changes on A_s extracted from the data on the central panel (dark blue circles) and fit to a first order kinetics (eq. S21, red trace). (b) idem to (a) for S1 sample using vesicles with 10% DODAB. The fit shown in the right side panel is to double exponential eq. S22. (c) idem to (b) for S2 sample. (d) Idem to (b) for S3 sample. (e) Idem to (b) for S4 sample. (f) Idem to (b) for S5 sample. (g) Idem to (b) for S6 sample.

2.7. On the apparent pH in the samples.

The ratio between the absorbance at 403 and 454 is very sensitive to changes in the pH around pH 7. We built up a calibration curve of these changes in our high-salt buffer (Supplementary Fig S4 (a) and (b)), which allowed us to monitor any changes in the pH during the course of the experiments. According to this ratio, there are differences in the apparent pH between different experiments. Thus, for experiments in the bulk (with or without vesicles present) the ratio corresponds to a pH of 7.2, as does for samples *S1* (**AP** confined in vesicles of 800 nm). In the rest of the samples, where spherical vesicles are used (*S2* to *S5*), the apparent pH takes values from 6.9 to 6.7, while in the osmotically shrunk vesicles (samples S6) the ratio suggests a pH of 6.4 (Supplementary Fig S4 (c)). The pH of the confined volume would decrease if the acidic product of the reaction (acetic acid) remains trapped within the cavity, in which case the reaction of hydrolysis would be also slowed down. The pH is however constant, showing that the acetic acid permeates the membrane, equilibrating the pH of the cavity with the exterior at a faster rate than that of the reaction of hydrolysis. The ratio of the absorbance does also depend on the polarity of the medium. For example, the ratio decreases when the percentage of MeOH in water increases. It has been shown that the polarity of the water membrane interface resembles that of mixtures water/methanol. We can therefore attribute the observed differences in the ratio to the different extent of binding of pyranine to the membrane in each of the samples (Supplementary Fig S4 (d)). From this observation it follows that pyranine leakage during the experiment would change the absorbance ratio, showing as an apparent increase in pH. The fact that the ratio (and the apparent pH) remains constant for all samples is consistent with the lasting integrity of the vesicles.

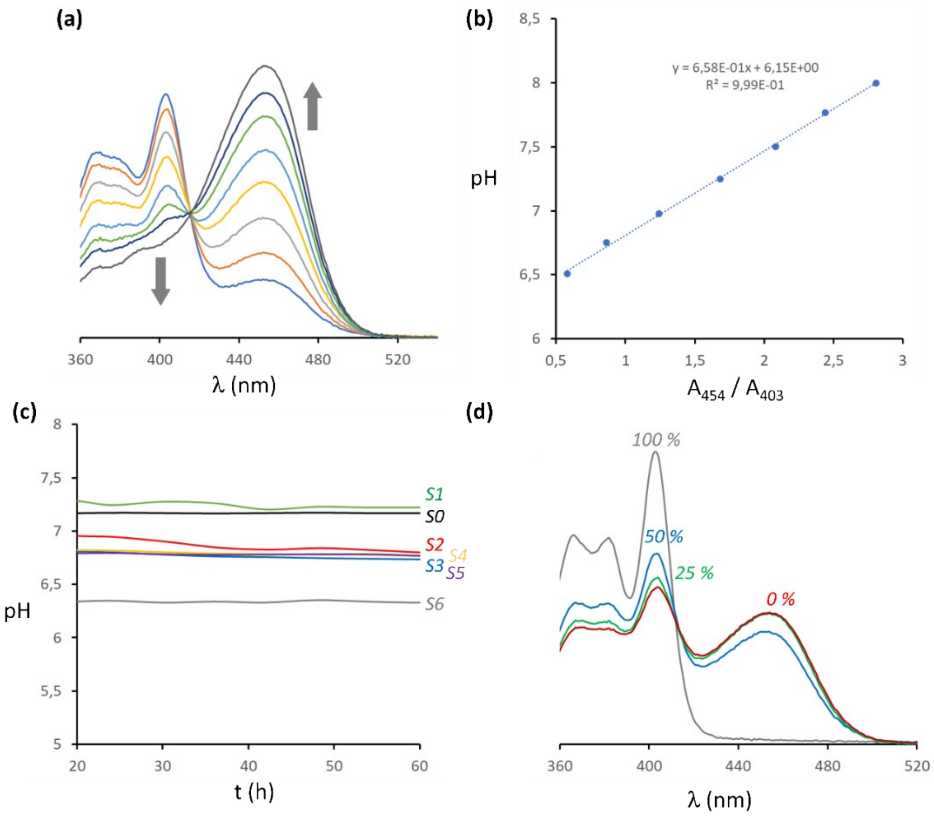

Supplementary Figure S4. (a). Changes in the UV spectrum of pyranine with the pH in high salt buffer. The concentration of pyranine was 20 mM. The pH of the buffer was changed by adding increasing amounts of a concentrated NaOH solution (5 M). The arrows indicate the direction of the changes, starting at pH 6.5 up to pH 8.0. (b). Correlation of the ratio of the absorbances at 454 over 403 nm, together with the linear fit. (c). Changes in the apparent pH of samples S0 to S6 with time. (d). Changes in the UV spectrum of pyranine (20 mM in high salt buffer, pH 7.2) as the percentage of MeOH (see labels) is increased.

2.8. Estimating the shape and size of osmotically shrunk vesicles.

We assume that the volume change in the cavity of the vesicles must compensate for the osmotic pressure difference between the bulk and the cavity. The osmotic pressure can be calculated using the van´t Hoff formula:

$$\Pi = \phi CRT \qquad \text{(S24)}$$

Where ϕ is the van´t Hoff index, which depends on the salt type and concentration used, and C is the concentration of all the ions that constitute the salt. Where there are different salts, we approximate the pressure as the sum of the contribution of all the different salts. That is, for salts a and b we have that:

$$\Pi = (\phi_a C_a + \phi_b C_b)RT \qquad \text{(S25)}$$

In the bulk solution we have sodium phosphate buffer, 100 mM, pH 7.2 and NaCl 2 M. From the phosphate we have the following concentration of ions:

$$\left[HPO_4^{2-}\right] = 0.05M$$

$$\left[H_2PO_4^-\right] = 0.05M$$

$$\left[Na^+\right] = 0.15M$$

The van't Hoof index for this salt at 37 C is 0.84.[31] Applying eq. S25 we have that the contribution of the phosphate to the osmotic pressure is 0.21RT. This is the initial osmotic pressure in the cavity of the vesicles and the bulk solution.

During the osmotic shock procedure, the concentration of phosphate is kept constant but that of NaCl is increased up to 2M (see Section 1).

Coming from the NaCl, we have the following concentration of ions:

$$\left[Na^+\right] = 2M$$

$$\left[Cl^-\right] = 2M$$

The van't Hoof index for this salt at 37 C is 0.99.[32] Applying eq. S25 we have that the contribution of the phosphate to the osmotic pressure in the bulk is 0.21RT, while the contribution of NaCl to the osmotic pressure in the bulk (Π_B) is 3.96RT. Globally, the osmotic pressure in the bulk is

$$\Pi_B = 4.17RT$$

The initial osmotic pressure in the cavity is that of the phosphate buffer, that is:

$$\Pi_{C,i} = 0.21RT$$

To equilibrate the osmotic pressures, the volume of the cavity needs to be reduced by a factor equivalent to the difference between the osmotic pressures in the cavity and in the bulk. Since changes in the bulk volume are negligible, the osmotic pressure in the shrunk cavity, Π_{SC}, should be that of the bulk, that is

$$\Pi_{SC} = 4.17RT$$

Assuming that only water permeates after osmotic shock, the increase in pressure is attributed to the reduction in volume to the same ratio, that is, the ratio of the final cavity volume, V_c, and that before shrinking $V_{c,i}$ should be:

$$\frac{V_{C,i}}{V_{SC}} = \frac{\Pi_{SC}}{\Pi_{C,i}} = 20 \qquad \text{(S26)}$$

In other words, the volume of the vesicle is shrunk 20 fold upon osmotic shock. It has been reported that lipid vesicles subjected to osmotic shrinking take a stomatocyte-like shape.[13] We start with the assumption that our vesicles undergo this type of transformation. The starting point are vesicles produced using extrusion via polycarbonate filters with a 400 nm pore, that produce vesicles with a radius of 110 nm according to DLS measurements. In a first approximation, we assume that during the formation of a stomatocyte-like structure the membrane folds into itself leading to a double-coated sphere, with a small *stoma* whose surface can be neglected in our calculations, or that ends up sealing-off, producing double-lamellar vesicles (Supplementary Fig. S5 (a)). From this assumption it follows that the membrane of the original vesicle is now folded into a double-membrane (Supplementary Fig S5) surrounding the cavity of the stomatocyte. That is, the original spherical vesicle has a

surface S_i, while the spherical stomatocyte has an external surface, S, approximately half the original surface , i.e.:

$$S = \frac{S_i}{2} \quad \text{(S27)}$$

Writing the surfaces as a function of the respective sphere radius and simplifying we have that the radius of the stomatocyte, *r*, and that of the original vesicle have the following relationship:

$$r = \frac{r_i}{\sqrt{2}} \quad \text{(S28)}$$

The total volume of the sphere defined by the stomatocyte, *V*, can be written as a function of the radius of the initial vesicle, r_i, as

$$V = \frac{4}{3}\pi r^3 = \frac{4}{3}\pi\left(\frac{r_i}{\sqrt{2}}\right)^3 \quad \text{(S29)}$$

Therefore, the ratio between the volume of the initial vesicle (V_i) and that of the sphere defined by the stomatocyte is:

$$\frac{V_i}{V} = \sqrt{2}^3 \quad \text{(S30)}$$

The volume confined within the boundaries of the membrane is the volume that remains between the two layers of the stomatocyte. This is the final volume, V_f, should be 20 times smaller than the volume of the initial vesicle, V_0, that is:

$$V_f = \frac{V_0}{20} \quad \text{(S31)}$$

In our stomatocyte-like structure, V_f can be approximated as the product of the surface of the sphere multiplied by the thickness of the inter-membrane layer, *t*, i.e.:

$$V_f = 4\pi r^2 t \quad \text{(S32)}$$

Thus, the value of *t* can be calculated as:

$$4\pi r^2 t = \frac{1}{20} \times \frac{4}{3}\pi {r_i}^3 \quad \text{(S33)}$$

Which can be simplified to:

$$t = \frac{{r_i}^3}{r^2 60} \quad \text{(S34)}$$

Substituting in eq. S28 we have that:

$$t = \frac{r_i}{30} \quad \text{(S35)}$$

Thus, for r_i = 110 nm, *t* is 3.7 nm, virtually identical to the thickness of the membrane 2*d* = 3,7 nm (Supplementary Figure S5(a)). Cryo-EM imaging of osmotically shrunk vesicles reveals a

dominant population of double-lamellar vesicles, an extreme version of stomatocytes that is consistent with the calculations above. See Supplementary Images File *EM_images* for a collection of 5 control samples (lipid vesicles from S2 samples) and 5 osmotically shrunk samples (lipid vesicles from S6 samples). In each of these images, vesicles with a single lamella are labelled with an "S", those with double lamella, with a "D". Multilamellar vesicles, which are present in both S2 and S6 samples, are not labelled and not taken into account for the statistical analysis. The images contain a 100 nm size bar and a small cartoon with 2 parallel lines (each line and the interline space 3.7 nm across) is also show superposed to all double-lamella vesicles, for reference. The summary of the structural analysis is shown in Supplementary Figure S5 (b).

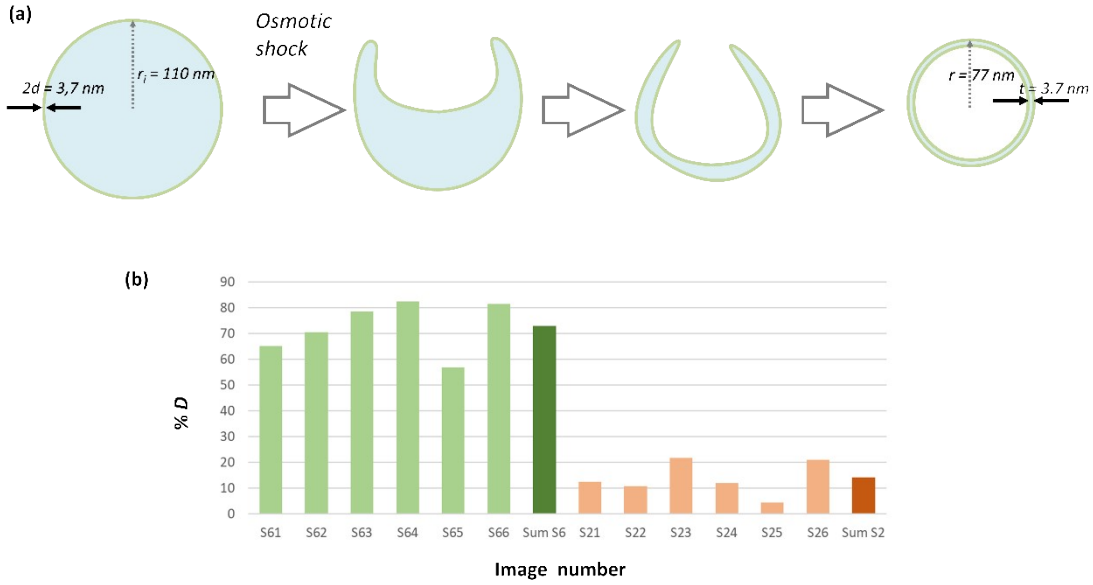

Supplementary Figure S5. (a) Scheme of a plausible process for the formation of extreme stomatocyte structures (in practice, double lamella vesicles with a thin inter-membrane volume) upon osmotic shock in our experiments. (b) Percentage of double lamella vesicles over the sum of double and single lamella vesicles, determined from EM images (See file *EM_images*).

3. Derivation of the model of confinement effect

3.1. Initial model

The confinement effect on hydrolysis (that is, the protection against hydrolysis of confined molecules) is attributed to the binding of the confined molecule to the membrane in an environment where the apparent membrane concentration is very large. We define an experimental confinement effect, C_e, that can be calculated as the ratio of the rate of hydrolysis in the bulk (k_b) over the ratio of hydrolysis of the confined molecule (k), that is:

$$C_e = \frac{k_b}{k} \qquad (1)$$

In the first instance, we derive a theoretical model that relates the C_e to the size of the radius of a spherical vesicle. We start the process by defining the degree of membrane binding of **AP**, α, as:

$$\alpha = \frac{[AP \cdot L]}{[AP]_0} \qquad (S36)$$

Where [**AP**·L] is the concentration of membrane-bound **AP** and $[\mathbf{AP}]_0$ is the total concentration of vesicle confined **AP**.

The dissociation constant, K_d, of **AP** from the membrane is:

$$K_d = \frac{[AP][L]_C}{[AP \cdot L]} \quad \text{(S37)}$$

Where $[L]_c$ is the apparent concentration of lipids in the cavity. The mass balance of **AP** is:

$$[AP]_0 = [AP \cdot L] + [AP] \quad \text{(S38)}$$

Combining eqs. S36, S37 and S38 we have that:

$$K_d = \frac{(1-\alpha)[L]_C}{\alpha} \quad \text{(S39)}$$

which can be re-arranged to:

$$\alpha = \frac{[L]_C}{K_d + [L]_C} \quad \text{(4)}$$

Vesicle confined **AP** is found either in the aqueous cavity or bound to the membrane. The fraction on the aqueous cavity undergoes hydrolysis with rate constant k_b, while that bound to the membrane, with the rate constant for membrane-bound **AP**, k_m. The observed rate constant is the weighted average of these two rate constants, and can be written as:

$$k = (1-\alpha)k_b + \alpha k_m \quad \text{(3)}$$

By substituting eq. 4 in eq. 3 we can write the rate constant as a function of the concentration of lipids in the cavity, e.g.:

$$k = k_b + \frac{(k_m - k_b)[L]_C}{K_d + [L]_C} \quad \text{(S40)}$$

Which can be re-arranged to:

$$k = \frac{k_b K_d + k_m [L]_C}{K_d + [L]_C} \quad \text{(S41)}$$

Substituting eq. S41 in eq. 1 we have that:

$$C_e = \frac{k_b K_d + k_b [L]_C}{k_b K_d + k_m [L]_C} \quad \text{(S42)}$$

And substituting Eq. 2 in, C_e can be written as a function of the vesicle radius:

$$C_e = \frac{k_b K_d + 3k_b / a_L r n_A}{k_b K_d + 3k_m / a_L r n_A} \quad \text{(S43)}$$

Re-arranging eq. S43 we have that:

$$C_e = \frac{3k_b + n_A a_L k_b K_d r}{3k_m + n_A a_L k_b K_d r} \quad \text{(5)}$$

Eq. 5 represents our initial theoretical model and was used to build the grey traces in Fig. 3 and Supplementary Fig. S6. We used k_b as calculated from the hydrolysis of non-confined **AP** (sample S0).

In osmotically shrunk vesicles, the concentration of lipid is 1.34 M. With a K_d value of 31 mM (e.g., the weakest affinity for the membrane calculated for **AP**) the value of α is 0.98 and for 13 mM (the strongest affinity for the membrane calculated for **AP**) is 0.99. It is therefore reasonable to take the rate constant of hydrolysis of **AP** in these vesicles as k_m, and this value was imputed in Eq. 5. α_m was 0.67 $nm^2 molec^{-1}$.[37]

3.2. Incorporating the packing parameter in the model.

The packing parameter *P* has been defined as:[34]

$$P = \frac{V_h l_h}{a_i} \qquad \text{(S44)}$$

Where a_i is the area occupied by the polar region of the lipid, V_h is the volume of the hydrophobic section and l_h its length. V_h can be approximately written as the product area of the lipid at the end of the lipid tail, opposite to the polar headgroup, a_m, and the hydrophobic length, i.e.:

$$V_h = a_m l_h \qquad \text{(S45)}$$

Substituting eq. S45 in eq. S44 we have that;

$$P = \frac{a_m}{a_i} \qquad \text{(6)}$$

we define the membrane packing parameter, P_M as:

$$P_M = \frac{s_m}{s_i} \qquad \text{(7)}$$

Where s_m is the surface area of the membrane at the mid-membrane depth and s_i the internal surface area (Fig 3(a)).

The total inner surface covered by the headgroups, $s_{i,h}$, is

$$s_{i,h} = n_{L,c} a_i \qquad \text{(S46)}$$

where $n_{L,c}$ is the number of lipid molecules in the inner leaflet of the membrane. The total surface of the packing defects, s_d, is the difference between the total surface of the membrane minus the surface covered by the headgroups, i.e.:

$$s_d = s_i - n_{L,c} a_i \qquad \text{(S47)}$$

The fraction of defects is therefore:

$$x_d = \frac{s_i - n_{L,c} a_i}{s_i} \quad \text{(S48)}$$

Dividing by s_m the numerator and denominator we have:

$$x_d = \frac{s_i/s_m - n_{L,c} a_i/s_m}{s_i/s_m} \quad \text{(S49)}$$

And substituting in eq. 7 we have that

$$x_d = \frac{1/P_M - n_{L,c} a_i/s_m}{1/P_M} \quad \text{(S50)}$$

The total surface at the mid-plain of the membrane is the sum of the surface all lipid surfaces at the mid-plane, that is

$$s_m = n_{L,c} a_m \quad \text{(S51)}$$

Substituting in eq. S51 we have that:

$$x_d = \frac{1/P_M - a_i/a_m}{1/P_M} \quad \text{(S52)}$$

Substituting in eq. 6 and rearranging we have that:

$$x_d = 1 - \frac{P_M}{P} \quad \text{(S53)}$$

For a flat membrane, we have that $s_i = s_m$, that is, $P_M = 1$. Therefore, x_d for a flat membrane, $x_{d,f}$, is:

$$x_{d,f} = 1 - \frac{1}{P} \quad \text{(8)}$$

For simplicity of calculation, we normalize x_d so that it adopts a value of 1 when the membrane is flat. Thus, normalised x_d, $x_{d,N}$, is:

$$x_{d,N} = \frac{x_d}{x_{d,f}} = \frac{P - P_M}{P - 1} \quad \text{(S54)}$$

P_M can be written as a function of the radius r (i.e., measured from the vesicle centre and the mid-membrane plane, Fig 3(a)) and the half-thickness of the membrane d (Fig 3(a)) as follows:

$$P_M = \frac{4\pi r^2}{4\pi (r-d)^2} = \frac{r^2}{(r-d)^2} \quad \text{(S55)}$$

Combining with eq. S54, we have that:

$$x_{d,N} = \frac{P}{(P-1)} - \frac{r^2}{(r-d)^2 (P-1)} \quad \text{(S56)}$$

We assume that the concentration of defects in the membrane equals that of lipids for a flat membrane. Therefore, the concentration of defects in the cavity, $[D]_C$, can be written as a function of the normalized fraction of packing defects as:

$$[D]_C = x_{d,N}[L]_c \quad \text{(S57)}$$

Combining with eqs. S57, S56 and 2 we have:

$$[D]_C = \left(\frac{P}{(P-1)} - \frac{r^2}{(r-d)^2\,(P-1)}\right)\frac{3}{a_m r.n_A} \quad \text{(S58)}$$

That can be re-arranged as:

$$[D]_C = \frac{3P}{n_A A_L (P-1) r} - \frac{3r}{n_A A_L (r-d)^2\,(P-1)} \quad \text{(S59)}$$

We assume that each defect is a binding site for **AP**. The corresponding dissociation constant can be written as:

$$K_d = \frac{[D][AP]}{[AP \cdot D]} \quad \text{(S60)}$$

Were [*D*] is the concentration of free defects in the membrane and [**AP**·*D*] that of defects-**AP** complexes. In contrast with the previous simpler model of membrane binding in the cavity, we cannot now assume that the concentration of lipid (or defects) is much larger than that of **AP**, as their amount decreases drastically within the cavity of very small vesicles. We need therefore to consider both the mass balance of **AP** and that of the defects in our calculations, i.e.:

$$[AP]_0 = [AP \cdot D] + [AP] \quad \text{(S61)}$$

$$[D]_C = [AP \cdot D] + [D] \quad \text{(S62)}$$

Combining eqs. S60, S61 and S62 we have that:

$$K_d = \frac{([D]_C - [D])([AP]_0 - [AP \cdot D])}{[AP \cdot D]} \quad \text{(S63)}$$

Re-arranging, we have that:

$$[AP \cdot D] = \frac{[AP]_0 + [D]_C + K_d - \sqrt{([AP]_0 + [D]_C + K_d)^2 - 4[AP]_0 K_d}}{2} \quad \text{(S64)}$$

The fraction of **AP** bound is α, i.e.:

$$\alpha = \frac{[AP \cdot D]}{[AP]_0} \quad \text{(S65)}$$

Substituting in eq. S64 we have that

$$\alpha = \frac{[AP]_0 + [D]_C + K_d - \sqrt{([AP]_0 + [D]_C + K_d)^2 - 4[AP]_0 K_d}}{2[AP]_0} \quad \text{(S66)}$$

The overall model is therefore composed of the following system of equations:

$$[D]_c = \frac{3P}{n_A a_m (P-1) r} - \frac{3r}{n_A a_m (r-d)^2 (P-1)} \quad \text{(S59)}$$

$$\alpha = \frac{[AP]_0 + [D]_C + K_d - \sqrt{([AP]_0 + [D]_C + K_d)^2 - 4[AP]_0 K_d}}{2[AP]_0} \quad \text{(S66)}$$

$$k = (1-\alpha)k_b + \alpha k_m \quad (3)$$

$$C_e = \frac{k_b}{k} \quad (1)$$

In which C_e is the dependent variable and r the independent variable. All the parameters except P and K_d were entered as known constants during the fitting procedure (Table 2, Fig. 3(b) and Supplementary Fig. S6).

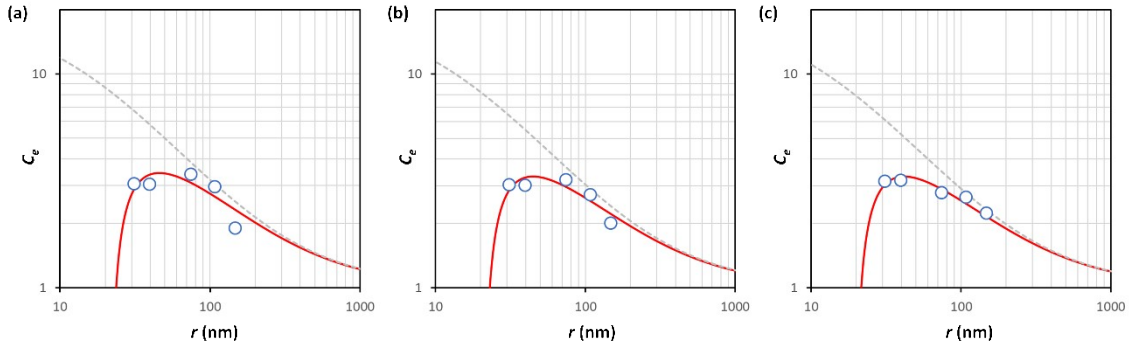

Supplementary Figure S6. (a) Fitting of experimental C_e with 0% DODAB lipid in the membrane, to the confinement model that incorporates the packing defects. (b) Idem for lipid vesicles with 2.5% DODAB. (c) Idem for lipid vesicles with 5% DODAB. The grey dashed traces represent the theoretical changes of C_e in the absence of a membrane packing effect on **AP** binding to the membrane (e.g., according to Eq. 5).

Supplementary references

1S. M. Sharma, D. V. Mhaske, M. Mahadik, S. S. Kadam, S. R. Dhaneshwar. *Indian J. Pham. Sci.*, **2008**, *70*, 258.